Received January 15, 2021, accepted February 16, 2021, date of publication February 24, 2021, date of current version March 4, 2021.

Digital Object Identifier 10.1109/ACCESS.2021.3061761

Effect of Data Pre-Processing on the Performance of Neural Networks for 1-D Transient Electromagnetic Forward Modeling

MUHAMMAD RIZWAN ASIF[1,2], THUE S. BORDING[1], ADRIAN S. BARFOD[2], DENYS J. GROMBACHER[1], PRADIP K. MAURYA[1], ANDERS V. CHRISTIANSEN[1], ESBEN AUKEN[3], AND JAKOB J. LARSEN[2], (Senior Member, IEEE)

[1]HydroGeophysics Group (HGG), Department of Geoscience, Aarhus University, 8000 Aarhus, Denmark
[2]Department of Electrical and Computer Engineering, Aarhus University, 8200 Aarhus, Denmark
[3]Geological Survey of Denmark and Greenland (GEUS), 1350 Copenhagen, Denmark

Corresponding author: Muhammad Rizwan Asif (rizwanasif@geo.au.dk)

This work was supported in part by the Innovation Fund Denmark under the ''MapField'' project and in part by ''TopSoil'', an Interreg project supported by the North Sea Programme of the European Regional Development Fund of the European Union through the tTEM data from Søften and in part through the tTEM data from Gedved by ''TREX'', a project supported by a Grønt Udviklings- og Demonstrations Program (GUDP) under ministry of food agriculture and fisheries of Denmark (Grant No. 34009-18-1453).

ABSTRACT Geophysical modelling and data inversion are important tools for interpreting the physical properties of Earth's subsurface. Solving the inverse problem involves several computational steps and is generally a time consuming task. Artificial neural networks have the potential to speed up large computations. Such networks provide the means to model the relationship between the inputs and outputs without needing to know the physical model of the underlying problem. There are two main aspects that affect the performance of neural networks: optimization of network architecture and pre-processing of data. In this article, we investigate several traditional pre-processing techniques including the min-max scaling, z-score scaling, and the logarithmic transform scaling, and propose some novel data pre-processing approaches for the 1-D forward modelling of time-domain electromagnetic data based on signal characteristics. We evaluate the performance of the conventional and the proposed pre-processing methods against a 3% relative error metric, which corresponds to the typical data uncertainty, to show that forward data pre-processing has significant effect on the performance of neural networks. The proposed gate-wise min-max scaling achieves the best performance with 96% of gates within a 3% relative error, while the commonly used logarithmic transform results only in 75% of gates within a 3% relative error. We provide insights into how various pre-processing methods affect the performance of these networks and recommend optimal pre-processing strategies that may be used where similar data content is encountered to achieve superior performance. Finally, we show the effect of forward modelling accuracy in inverse modelling.

INDEX TERMS Data normalization, data pre-processing, forward modelling, inverse modelling, neural networks.

I. INTRODUCTION

Geophysics is an important tool for guiding predictions about the geology of the subsurface of the Earth. The geophysical workflow begins with the collection of data and ends with a model of subsurface properties. The process of translating the observed data into a parameterized model of the subsurface is often referred to as inversion and is a challenging problem. Solving an inverse problem usually requires probabilistic or deterministic methodologies that are computationally expensive and require extensive processing power for large surveys.

In order to speed up the inversion process, neural networks can be used for two different mechanisms: (a) as a fast emulator for the forward problem, (b) as a mechanism to directly estimate a resistivity model given data. Such networks provide the means to model the relationship between the inputs and the target outputs without needing to know the underlying principle of the physical model. During an inversion, forward modelling, predicting data from a proposed model, is computed repeatedly, hence a speed-up in this process can

The associate editor coordinating the review of this manuscript and approving it for publication was Giovanni Angiulli.

have significant impact on the overall performance of the inversion process. Therefore, neural networks have been used for the simulation of, e.g., forward modelling for borehole resistivity measurements [1], electromagnetic induction data [2], [3], and seismic waveform inversion [4]. To avoid the heavy repetitive process of computing forwards during inversion, neural networks have also been used directly for seismic impedance inversion [5], electrical resistivity imaging inversion [6], inversion of electromagnetic data [7]–[9], and magneto-telluric inversion [10].

Many of these previous works have achieved promising results. However, they have mainly focused on the neural network's architecture and its configuration, including type of network, number of neurons, convolution kernel size, loss function, activation function, the depth of network, etc. In order to surrogate a physics-based model, it is imperative to extract maximum precision from the network. Errors in the network's output will propagate to the inversion process and culminate in more or less erroneous models.

Several studies on the effect of data pre-processing, also referred to as data normalization, for various applications outside geophysics show that it substantially affects the network's performance [11]–[15]. Data pre-processing is essential for geophysical data where the numerical data values may span several orders of magnitude. One particular example dealt with here is TEM data, where the dynamic range of the data easily spans four to six orders of magnitude [16]. TEM data is used to map the spatial variation of electrical resistivity of the subsurface, which reflects variation in the geological structures.

In this article, we specifically focus on the 1-D forward data pre-processing and investigate several schemes preceding the approximation of forward responses of a TEM system using artificial neural networks. We show that the choice of data pre-processing significantly affects the performance of a neural network and a substantial improvement in accuracy can be achieved if optimal pre-processing strategy is used. This investigation is based on data from the towed TEM instrument, called tTEM [17] and 1-D Earth model is considered. The network input is the subsurface 1-D resistivity model and the distance between the transmitter and receiver coil. The target output of the network is the numerically computed magnitude of the forward response produced for a step-response TEM calculation, i.e., the B-field. We compare the accuracy performance of the trained neural network for the different pre-processing methods and provide insights into how these methods affect the performance of the neural network forward responses. We show that more variation in data curves consequently results in better performance. We also show that a significant speed-up can be achieved by using the neural network based forward modelling with insignificant loss of accuracy. We also present the effects of forward modelling accuracy in inverse modelling. Although, we have used the data from the tTEM system, the proposed approaches could be used for any TEM system, airborne or ground-based, yielding similar data.

The rest of the article is structured as follows. We present the investigated pre-processing schemes and the deployed neural network configuration in Section II. In Section III, we discuss the results and provide insights into how the presented pre-processing methods affect the performance of neural networks. We also show the effect of forward modelling accuracy in inverse modelling in Section III. In Section IV, we discuss the limitations and prospects. Lastly, in Section V, we give the concluding remarks.

II. PROPOSED METHODOLOGY

TEM methods are used to image the spatial variation of the electrical resistivity, or equivalently the conductivity, of the subsurface, where electrical patterns typically reflect geological structures. The tTEM system is a system specifically designed for detailed geophysical mapping of the shallow subsurface, which is required for many applications including aquifer vulnerability mapping [18], assessing locations of artificial recharge sites [19], and nitrate retention mapping [20]. It uses a 2 m $\times$ 4 m transmitter coil and a z-component receiver coil in an offset configuration. The distance between the receiver and transmitter coil is usually fixed around 9 m, but this may vary when the system is re-configured or re-deployed. The system is towed by an all-terrain vehicle.

During the forward modelling, a predicted TEM response of a given resistivity model is calculated using a numerical algorithm. On the contrary, inverse modelling starts with the observed geophysical data and aims to produce a model in agreement with those data. The inversion is an iterative refining of an initial subsurface model until an optimal model is realized. The iterative procedure is continued until the predicted data from the forward response of the subsurface model and the observed data agree within some threshold values. This iterative process is computationally intensive, and most of the time is spent during the computation of the Jacobian matrix, where a significant number of forward responses are computed.

In order to examine the effects of data pre-processing on the performance of neural networks, we choose to investigate the relationship from 1-D model to data space, i.e. the forward modelling. While it is possible to use neural networks directly for transforming measured data to a model, it would require training on the data affected by the transmitter waveform and receiver coil characteristics, which may vary between surveys, and re-training would be required. However, the effect of the system response can be applied as a convolution. Therefore, by applying the neural network for the forward response directly from step-response, we can make the process widely applicable, and use the well investigated inversion algorithms [21].

A. DATA PRE-PROCESSING

It is challenging to achieve the desired performance without normalizing or pre-processing the geophysical response

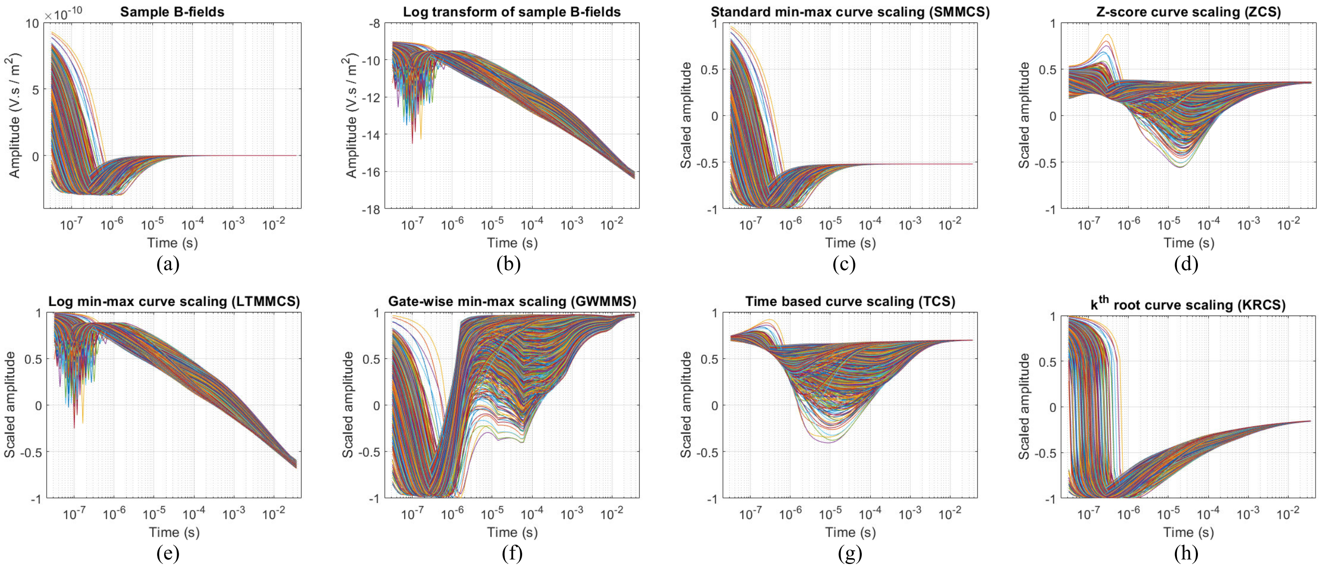

FIGURE 1. **Visualization of un-processed and processed B-fields of a subset of data used in this study. (a) Raw target outputs. (b) Raw target outputs in log space. (c) Standard min-max curve scaling (SMMCS). (d) Z-score curve scaling (ZCS). (e) Logarithmic transform min-max curve scaling (LTMMCS). (f) Gate-wise min-max scaling (GWMMS). (g) Time based curve scaling (TCS). (h) Kth root curve scaling (KRCS).**

prior to training the neural network. The raw data amplitudes span several orders of magnitude and the larger data values would have a larger impact in the loss function than smaller values [22]. Hence, the distribution of data is significant as it can directly affect the performance of neural networks. Therefore, it is necessary to perform data pre-processing, also known as data normalization or standardization, when neural networks are deployed [13]. For the case of tTEM, the inputs consist of the distance between the transmitter and receiver coil and 30-layer 1-D resistivity models with logarithmically increasing thicknesses with a top layer thickness of 1 m and a depth to last layer boundary at 120 m. The layer thicknesses are fixed and not considered as input parameters.

The target outputs are the predicted TEM forward responses for the corresponding resistivity models, i.e., magnitude of the secondary magnetic field, the B-field, produced from a step-response. A well-known code [21] is used to calculate the numerical responses. The 1-D forward responses are generated at 86 discrete time intervals or "time gates" from 30 ns till 30 ms with logarithmically increasing gate widths sampled at 14 gates/decade. Although the typical TEM data range is narrow, a wider range is considered in order to obtain an accurate response after convolution with the system response.

1) NEURAL NETWORK INPUT PRE-PROCESSING

It is practical to consider logarithmic variations in resistivity, as the response of the forward model does not vary linearly with resistivity. For example, a resistivity change from 10 Ω·m to 20 Ω·m would affect the data space more than a change from 110 Ω·m to 120 Ω·m. Therefore, we apply the logarithmic transform on the resistivity model before scaling it between $[a, b]$ using (1).

$$\mathbf{R}_n = a + \frac{(b-a)\left(\log_{10}(\mathbf{R}) - \log_{10}(R_{\min})\right)}{\log_{10}(R_{\max}) - \log_{10}(R_{\min})} \tag{1}$$

where $\mathbf{R}_{\mathrm{n}}$ is the normalized resistivity model of $\mathbf{R}$, R_{min} and R_{max} denotes the global minimum and maximum resistivity values, both obtained from the training dataset.

The distance between the transmitter and receiver coil is usually fixed for a particular survey. It is normalized by the standard min-max scaling as in (2).

$$d_n = a + \frac{(b-a)(d - d_{\min})}{d_{\max} - d_{\min}} \tag{2}$$

where d_n and d are the normalized and actual distance between the transmitter and receiver respectively, while d_{min} and d_{max} are the minimum and maximum possible distances with values, i.e., between 7 m and 10 m in our case.

Therefore, the input to the network becomes as in (3):

$$\mathbf{I}_n = \begin{bmatrix} d_n \\ \mathbf{R}_n \end{bmatrix} \tag{3}$$

2) TARGET OUTPUT PRE-PROCESSING

The network target output, i.e. the B-field, has a dynamic range spanning several orders of magnitude. The gate values of the B-field are close to zero at late times. This is shown in Fig. 1(a) where the forward responses of 5978 resistivity models acquired from a survey are displayed. At late times, the amplitudes are close to zero and would contribute very little when the network is trained, unless special precautions are considered during pre-processing or in the loss function. Only small changes are observed in the curves after 10 μs, the changes being almost indistinguishable in linear space. Differences between curves are readily apparent in logarithmic space, shown in Fig. 1(b), where the logarithm of absolute data values are plotted. This suggests an advantage of using the logarithmic transform. However, it may have its disadvantages especially for systems with an offset configuration where data containing sign changes will be present. The performance of neural networks for TEM data is not only affected by the changes within a data curve, but also by the degree of variation between the observed data curves. Therefore, the un-processed or the standard pre-processing techniques may not perform well with geophysical data. Hence, in this section, we discuss several pre-processing techniques for the B-field and describe how one pre-processing may be better than the others for data-driven models based on TEM data.

3) STANDARD MIN-MAX CURVE SCALING (SMMCS)

A common machine learning pre-processing technique is the min-max scaling, which maps the data values between a specified range, ranging from the minimum value a to the maximum value b. This technique is often used with neural networks.

$$B_{SMMCS}(t) = a + \frac{(b-a)\,(B(t) - B_{\min})}{B_{\max} - B_{\min}} \tag{4}$$

where $B_{SMMCS}(t)$ are the normalized gate values for $B(t)$ while B_{min} and B_{max} are the global minimum and maximum value of the B-field.

4) Z-SCORE CURVE SCALING (ZCS)

Another standard machine learning data pre-processing technique is the z-score pre-processing where the observed data points are transformed to a common scale. This is achieved by subtracting the mean of each gate with the observed gate value and dividing it by the standard deviation of each gate as in (5). The transformed data values are then mapped between the desired range $[a, b]$ using (6).

$$B_{ZC}(t) = \frac{B(t) - B_m(t)}{B_s(t)} \tag{5}$$

$$B_{ZCS}(t) = a + \frac{(b-a)\,(B_{ZS}(t) - B_{ZS\,\min})}{B_{ZS\,\max} - B_{ZS\,\min}} \tag{6}$$

Here $B_{ZCS}(t)$ are the scaled gate values of the z-score normalized B-field $B_{ZS}(t)$. The mean and standard deviation at each gate time t are represented by $B_m(t)$ and $B_s(t)$ obtained from the training data curves, and B_{ZSmin} and B_{ZSmax} are the global minimum and maximum gate values observed at any gate time in the training set.

ZCS results in considerable variation in the data curves as shown in Fig. 1(d), and is expected to perform better as compared to SMMCS. This pre-processing technique changes the pattern of the original data curves, but results in smooth outputs.

5) LOGARITHMIC TRANSFORM MIN-MAX CURVE SCALING (LTMMCS)

Due to the minuscule change in late times in the raw data curves (see Fig. 1a), the logarithmic transform is used to visualize the data. This stretches the data and increases the emphasis on small values while decreasing the emphasis on large values. However, the logarithmic transform is not well-suited to data containing sign changes, which are often encountered in offset transmitter-receiver geometries or in the presence of induced polarization effects. As tTEM has an offset configuration, we consider this transformation on absolute data values as in (7) where the B-field is transformed into logarithmic space and then mapped to the desired range $[a, b]$ using (8).

$$B_{LT}(t) = \log_{10}(|B(t)|) \tag{7}$$

$$B_{LTMMCS}(t) = a + \frac{(b-a)\,(B_{LT}(t) - B_{LT\,\min})}{B_{LT\,\max} - B_{LT\,\min}} \tag{8}$$

where $B_{LTMMCS}(t)$ are the normalized gate values of $B_{LT}(t)$, while B_{LTmin} and B_{LTmax} are the minimum and maximum value encountered in $B_{LT}(t)$ at any gate time t.

The prediction error is expected to rise after post-processing, when data values are reverse transformed to raw values as this transform effectively stretches the dynamic range of the small values, while shrinking the dynamic range of large values. For simplicity, we use the absolute data values for comparison. If this transform is to be used, one or several additional parameters corresponding to the zero-crossings need to be added as output variables during training in order to be able to reverse transform the prediction data with sign changes.

6) GATE-WISE MIN-MAX SCALING (GWMMS)

To ensure variation in the data curves, we also propose to scale each gate value of the B-field between $[a, b]$ according to the maximum and minimum value of each respective gate in the entire set of training data curves using (9).

$$B_{GWMMS}(t) = a + \frac{(b-a)\,(B(t) - B_{\min}(t))}{B_{\max}(t) - B_{\min}(t)} \tag{9}$$

Here $B_{GWMMS}(t)$ are the normalized gate values, while $B_{min}(t)$ and $B_{max}(t)$ are the minimum and maximum gate values for each gate time t respectively obtained from the training data.

Gate-wise scaling ensures that each gate value is weighted equally and contributes equally during the training of the network. However, Fig. 1(f) shows that this transform distorts the shape of the data curve, especially after 10 μs.

7) TIME-BASED CURVE SCALING (TCS)

In order to incorporate more variation in the data at late times, we use (10) to transform the target output, which also results in a smooth curve. Then, the transformed curve is scaled in the specified range using (11) for training.

$$B_T(t) = B(t) \times t \tag{10}$$

$$B_{TCS}(t) = a + \frac{(b-a)\,(B_T(t) - B_{T\,\min})}{B_{T\,\max} - B_{T\,\min}} \tag{11}$$

where $B_{TCS}(t)$ is the transformed target output while B_{Tmin} and B_{Tmax} are the global minimum and maximum value encountered in $B_T(t)$ at any gate time t.

TCS results in significant variation in the data curves similar to ZCS as shown in Fig. 1(g) and Fig. 1(d). In comparison with ZCS, the variation from TCS is less at early times and is slightly more from 1 μs to 1 ms and results in smoother curves.

8) K-ROOT CURVE SCALING (KRCS)

We also transform the B-field curves by applying the kth root as in (12). To keep the negative data while transforming the original curve, only odd values of k are considered. The root transformed curve is then scaled to the desired range by (13).

$$B_R(t) = \sqrt[k]{B(t)} \tag{12}$$

$$B_{KRCS}(t) = a + \frac{(b-a)\,(B_R(t) - B_{R\,\min})}{B_{R\,\max} - B_{R\,\min}} \tag{13}$$

where $B_R(t)$ is the root transformed data curve while B_{KRCS} is the kth root scaled curve. The parameters $B_{R\min}$ and $B_{R\max}$ are the minimum and maximum values encountered in $B_R(t)$ at any gate time t in the training set. Essentially, the scaled output for any odd root results in a similar pattern. Hence, we consider KRCS for $k = 5$.

The transformed curve shown in Fig. 1(h) results in larger variation at early times as compared to the original curves while keeping the smoothness. However, less range is encountered at late times.

B. NEURAL NETWORK CONFIGURATION

The purpose of this study is to evaluate the comparative performance between various pre-processing techniques and not to realize the optimal network configuration. Therefore, we deploy a simple network topology consisting of a single fully-connected hidden layer as shown in Fig. 2. We train several networks by logarithmically grid-searching the number of neurons n in the hidden layer to evaluate various pre-processing techniques.

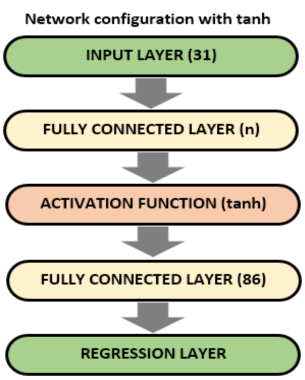

FIGURE 2. Neural network configuration with one hidden layer.

We have not considered the use of the state-of-the-art convolutional neural networks (CNNs) as they are primarily intended for data having a spatial relationship. The neural network configuration we have used is well-suited for predicting or mapping a real-valued quantity for a given set of inputs. This is in accordance with the universal approximation theorem [23], which states that a single fully connected hidden layer within the network containing a finite number of neurons can approximate any function under mild assumptions on the activation function. Additionally, CNNs are relatively more computationally expensive [24].

The input layer for the neural network consists of the normalized distance d_n between transmitter and receiver coil, and the 30 layer normalized resistivity model R_n as in (3). The output from the last fully-connected layer relates to the B-field having 86 outputs corresponding to each time gate. The range of $[a, b]$ for the inputs and the outputs is selected as $[-1, 1]$, and the hyperbolic tangent is considered as the activation function that also lies within the same range. It approaches -1 as the range goes to $-\infty$ and 1 when it goes to $+\infty$. Instead of randomly initializing the weights of the network, we deploy the Nguyen-Widrow initialization algorithm [25]. It approximately distributes the active region of each neuron in the layer evenly across the input space [26]. Small numbers of random values are assigned in the Nguyen-Widrow initialization prior to backpropagation, which helps reduce the time it takes to train a network [27]. The loss function in the regression layer is defined as the sum of squared errors (SSE) as in (14).

$$E = \sum_{i=1}^{N} \left(x_i - \widehat{x}_i\right)^2 \tag{14}$$

where x_i is the target output, $\widehat{x}_i$ is the predicted output and N is the number of samples.

The scaled conjugate gradient algorithm is used to update the network's weights and biases as it has no critical user-dependent parameters [28]. The only two required parameters are selected as $\sigma = 5 \times 10^{-5}$ that determines the change in weight for the second derivative approximation and $\lambda = 5 \times 10^{-7}$ that regulates the indefiniteness of the Hessian.

To avoid overfitting, which is very common in fully-connected networks, we apply an early stopping criterion. This ensures that the training is stopped when the validation loss starts to increase while the training loss may still be decreasing. We choose the validation check count to be 5000 epochs, which means that the training stops if the validation loss does not go lower than the best validation performance for the succeeding 5000 epochs. It is also explained in detail at a later stage in this article.

III. RESULTS

We have used MATLAB 2019b on a system with an Intel Xeon Gold 6132 CPU with 2.6GHz and four NVIDIA GeForce RTX 2080Ti GPUs. The training input comprises of randomly selected 100,000 resistivity models acquired from various tTEM surveys spread across Denmark. The model space covers a wide range of possible Danish geological environments. The validation and the test set, are comprised of two entirely different surveys conducted in Søften and Gedved, in central Denmark, containing a total of 697 and 5,978 resistivity models, respectively.

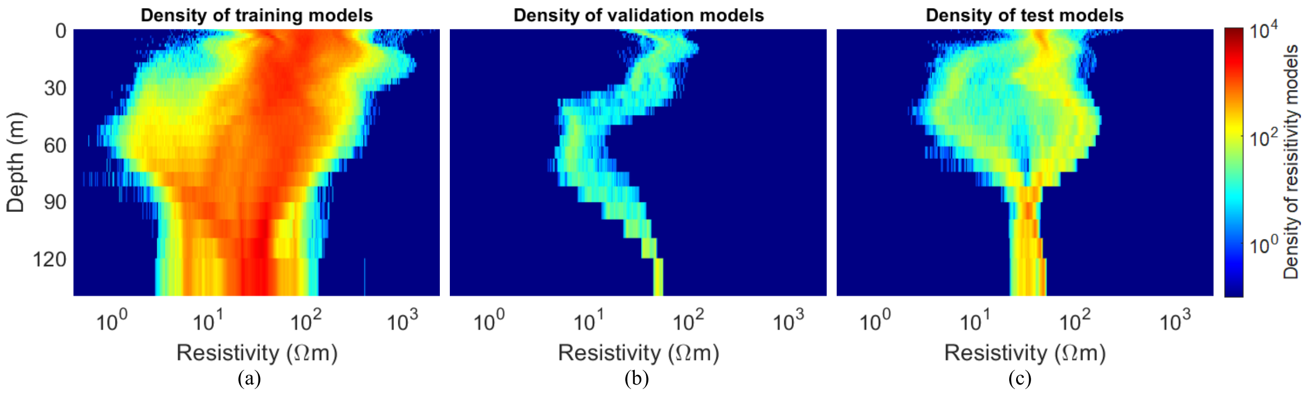

FIGURE 3. Density plots of resistivity models for training, validation and test sets (a) Training set. (b) Validation set i.e. the Søften survey models. (c) Test set, i.e. gedved survey models.

The validation and testing on different surveys provide a good measure of assessing the generalization of the network as those models are not encountered in the training set. However, it is important that they lie within the range of the training model space. The target test outputs, i.e., the forward responses, for the corresponding resistivity models are computed numerically. Figure 3 shows the range of resistivity values for the models used in this study. However, it does not show the variation of resistivity within each model.

The predicted outputs from the trained neural networks using the different pre-processing techniques are post-processed by reversing the corresponding pre-processing methodologies to transform the data back to the raw values for comparison with the numerical forward responses. For log-based pre-processing methods, we consider the results on absolute values of the B-field to reduce complexity.

As a 3% relative error is a typical data uncertainty in TEM systems, we use this as the metric for performance evaluation. Figure 4(a) shows the performance of different pre-processing methods versus the number of neurons for the test set. For most of the pre-processing approaches, the peak performance for a single hidden layer network is observed at $n = 384$. Therefore, Fig. 4(b) shows the cumulative percentage of gates with respect to the relative error for $n = 384$. We do not show the results of the validation set as it is only used to initiate the early stopping criterion. Figure 4(a) shows that the GWMMS achieves the best performance with 95.9% gates within the 3% relative error for n = 384. However, if the B-field curves are to be used to calculate the time derivative, dB/dt, errors will propagate and enlarge if the predicted curves are not smooth. Therefore, if the network target outputs are not smooth itself, the optimal performance may not be realized, and additional post-processing steps may be necessary.

It can be seen from Fig. 1(f) and Fig. 5(b) that the pre-processed target output for GWMMS does not result in a smooth curve and may require additional processing steps after post-processing back to raw data values. Nevertheless, this pre-processing strategy results in the best performance and could be used depending on the type of application. To increase the smoothness of the network output, one way is to incorporate an L_2 regularization term in the loss function. This term forces the network to have smaller weights and

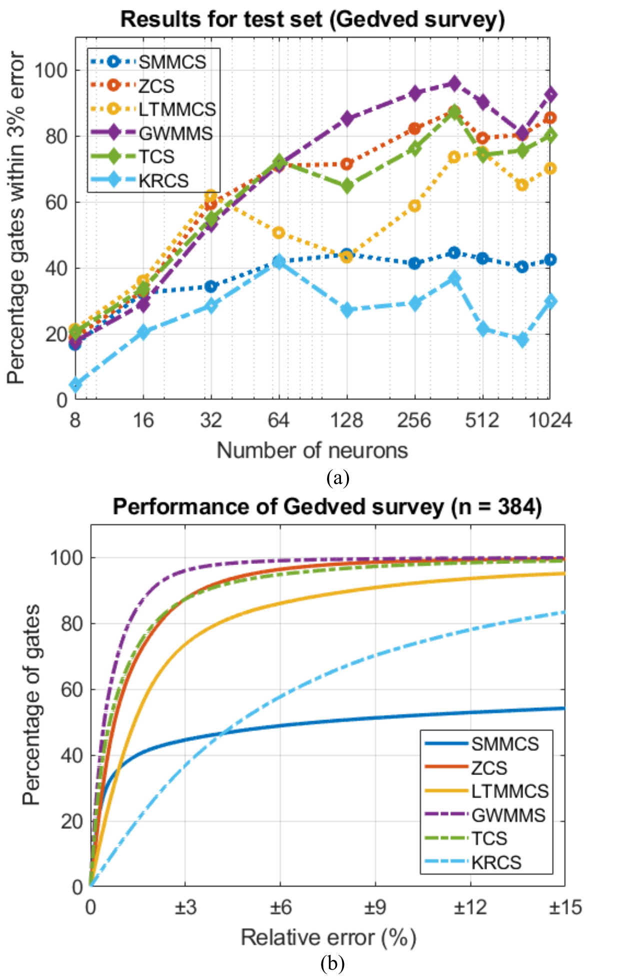

FIGURE 4. Performance of neural network for the test set (a) Percentage of gates within 3% relative error for different number of neurons in the hidden layer. (b) Cumulative sum of percentage gates with respect to relative error (%) for 384 neurons in the hidden layer.

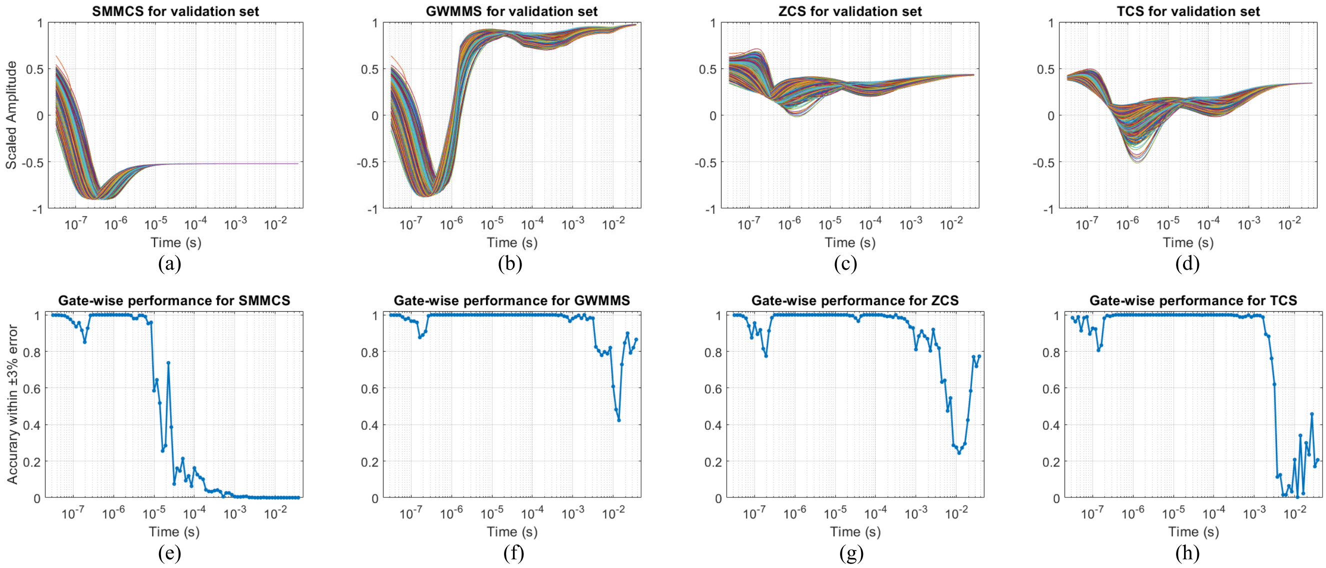

FIGURE 5. **Gate-wise accuracy within 3% relative error of SMMCS, GWMMS, ZCS and TCS for n = 384 for the validation set showing the effect of variation of data curves on performance (a) Target outputs for SMMCS. (b) Curves for GWMMS. (c) Target outputs for ZCS. (d) Curves for TCS. (e) Percentage gates within 3% relative error for SMMCS (f) Gate-wise performance for GWMMS. (g) Percentage gates within 3% relative error for ZCS. (h) Gate-wise performance for TCS.**

biases, which results in a smoother network response and most likely achieve a better generalization. An alternative way is to use the radial basis function network that results in smoother approximations [29], [30].

TCS and ZCS have almost identical overall performances and achieve the second-best accuracies resulting in 87.3% of all gates within the 3% relative error for $n = 384$. Figure 1(d) and Fig. 1(g) show that the pre-processed curves result in smooth outputs, which may have its advantages. The pre-processing based on the commonly used logarithmic transform in geophysics, i.e. the LTMMCS, results only in 75.0% of gates within a 3% relative error for $n = 512$ and 73.5% for $n = 384$. The error is reduced from 25% to 4.1% when the pre-processing is switched from LTMMCS to GWMMS and is dropped from 12.7% to 4.1% when switched from ZCS or TCS. Additionally, Fig. 4(b) also shows that GWMMS, ZCS and TCS pre-processing outperform the LTMMCS with a considerable margin. It can also be seen that SMMCS and KRCS give the worst accuracy performance. We ascribe this to the reduced variation in the curves at late times.

To illustrate the effect of data variation on the network's performance, we show the gate-wise accuracy for SMMCS and GWMMS within the 3% relative error in Fig. 5. It can be seen in Fig. 5(a) that the data variation of SMMCS is insignificant after 10 μs which consequently results in a poor performance for the gate times after 10 μs as shown in Fig. 5(e). Similarly, the GWMMS data variation starts to decrease after 1 ms as in Fig. 5(b), which correspondingly results in declined accuracy at late times as evident from Fig. 5(f).

As the overall accuracy of ZCS and TCS at $n = 384$ is found to be identical, we also show their gate-wise performance in Fig. 5. It can be seen from Fig. 5(c) and Fig. 5(d) that ZCS results in more variation in early times, therefore, resulting in better accuracy at early gates (see Fig. 5(g) and Fig. 5(h)). Similarly, more variation in TCS curves is observed from ~1 μs to ~2 ms and consequently, superior gate-wise performance is observed for TCS in that time range. Lastly, ZCS performs better for late times after ~2 ms as more variation is seen.

Overall, GWMMS achieves a superior performance as compared to other pre-processing techniques investigated in this study. However, as mentioned earlier, it may not be a viable solution if a smooth output is required from the network. In scenarios where a smooth output is required, deploying TCS may be a better strategy as its performance is superior to ZCS within usable gate times. The usable gate times typically begin from 5 μs to 100 μs and end around 1 ms to 3 ms for ground-based TEM systems.

We also show the loss function progress of GWMMS for $n = 384$ in Fig. 6, since it achieves the best performance. The best validation performance is achieved at epoch = 189,808 with an error of 0.2644. The validation loss does not decrease more than the best validation performance for the next consecutive 5000 epochs as shown in the inset of Fig. 6. This initiates the early stopping criterion and the network weights and biases are reset with the ones for which the best validation performance is achieved before the training is stopped. Since the number of samples in the training set is significantly larger than the validation set, the accumulation of errors for the training loss is higher than the validation loss.

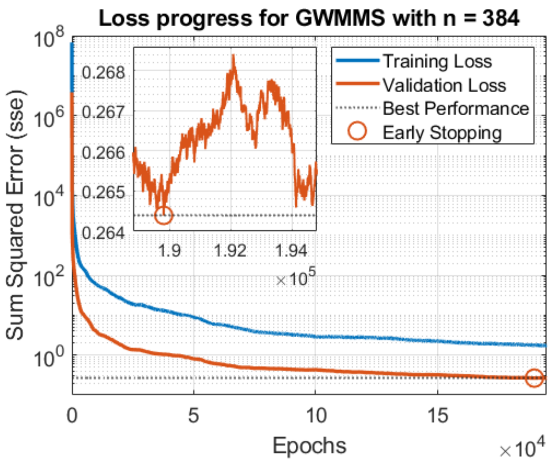

FIGURE 6. Loss function progress for the neural network with GWMMS for $n = 384$. Inset shows the validation loss progress for the last 6000 epochs that shows how early stopping criterion is applied.

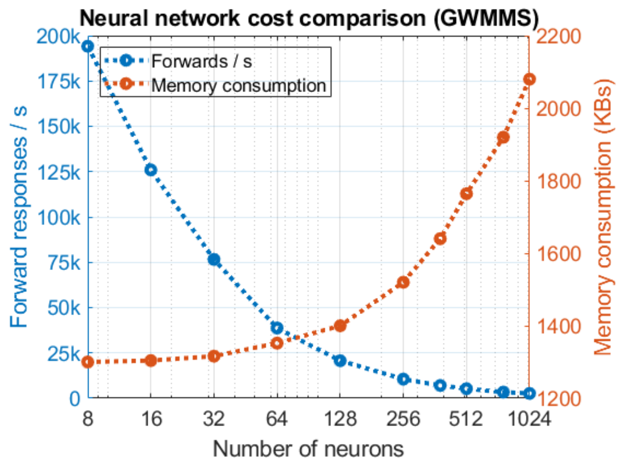

FIGURE 7. Computation time and memory consumption comparison for n number of neurons in a single layer feed forward neural network with GWMMS.

However, if the error is normalized, the training loss is lower than the validation loss.

The main motivation of this study is to speed-up the TEM forward modelling. Therefore, we compare the computation time of the neural network with GWMMS for $n = 384$ with two established geophysical modelling methods, namely AarhusInv [21] and AirBeo [31]. Both of these methods are implemented in FORTRAN, therefore, we perform the computational analysis on the same platform. It should be noted here that the computation time is evaluated on a single CPU core without any parallelization. Table 1 shows the comparison of the processing time of neural network based forward modelling with the typical modelling methods [21], [31]. Evident from Table 1, the neural network based approach is 400 times faster when compared to AarhusInv and almost 600 times faster when compared with AirBeo.

TABLE 1. Computation Time Comparison

Modelling Method	Speed
Proposed approach	7046.5 forward responses / s
AarhusInv [21]	16.2 forward responses / s
AirBeo [31]	11.8 forward responses / s

We also show the trend of computation time and memory consumption for n number of neurons with GWMMS for the network configuration we have used in this study (see Fig. 7). It can be seen that the computation time increases with the increase in the number of neurons. Additionally, the memory usage also increases. It should be noted here that the optimal network configuration may require a different network configuration, which would increase the computational time and memory usage for the proposed approach. However, it is still expected to perform significantly faster than the standard 1-D forward modelling codes. Hence, depending on the application, the pre-processing techniques achieving superior accuracy may be deployed for practical use after realizing the optimal network configuration for maximum performance.

We also exemplify the effects of data pre-processing on neural networks in inverse modelling with a genetic algorithm (GA) based inversion method [32]. We adapt the successfully deployed GA [33] for our case with the fitness function as in (15).

$$\phi(\mathbf{R}) = \frac{\left(\log_{10}\left(\mathbf{d_{syn}}\right) - \log_{10}\left(\mathrm{F}\left(\mathbf{R}\right)\right)\right)^2}{\left(\log_{10}\left(1+\sigma\right)\right)^2} \tag{15}$$

where $\mathbf{R}$ is the resistivity model, F is the neural network forward operator, $\mathbf{d_{syn}}$ is the data vector to be fitted, and σ is the noise level which is set to 3%.

Figure 8 shows an example of inversion on data of a synthetic model by using forwards generated from neural networks trained with SMMCS, GWMMS, ZCS and SMMCS for $n = 384$. Forward data from 5 μs to 3 ms is used which is the typical ground-based TEM time range. The model retrieved by using the forwards from the neural network trained on SMMCS, as shown in Fig. 8(a), significantly diverges from the synthetic model. This is due to the fact that the performance of SMMCS is satisfactory only from 5 μs to 10 μs (see Fig. 5(e)). These early times correspond to shallow information where the inverted model agrees fairly well with the synthetic model (down to 10-15 m in our case). In case of the forwards from the network trained using GWMMS, the inverted model agrees with the synthetic model down to 80-90 m (see Fig. 8(b)). This is in agreement with the forward accuracy of GWMMS where satisfactory performance is achieved from 5 μs to 1 ms as shown in Fig. 5(f). For the forwards from the network trained using ZCS, the inverted model agrees with the synthetic model down to 70-80 m as shown in Fig. 8(c). However, higher divergence is observed for deeper layers compared to GWMMS. This is expected since the forward accuracy of ZCS is lower at late times within usable gate times in comparison to GWMMS

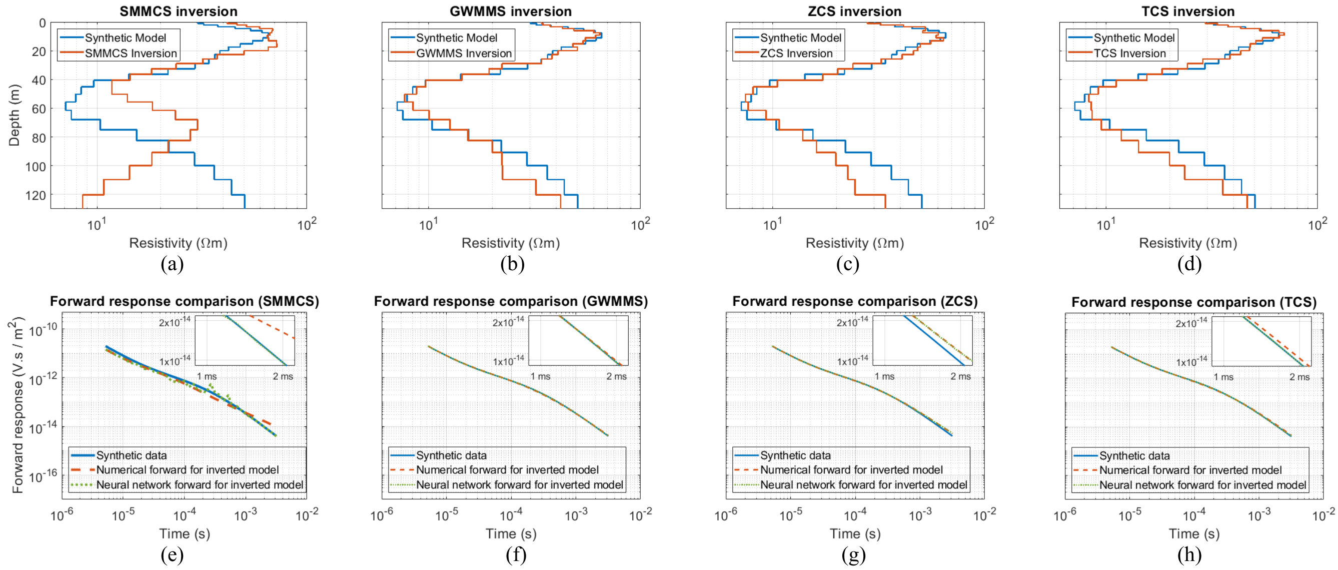

FIGURE 8. **Inversion and the corresponding forward response (from 5 μs to 3 ms) comparison of neural network trained on different pre-processing techniques with the numerical solution for a synthetic model. (a) Inversion using neural network trained by SMMCS. (b) GWMMS inversion. (c) Inversion by ZCS. (d) TCS inversion. (e) Comparison of numerical and neural network forward response for the inverted model from neural network trained using GWMMS where inset shows the forward response comparison from 1 ms to 2 ms. (f) GWMMS forward response comparison, inset shows forwards from 1 ms to 2 ms. (g) Forward response comparison of inverted model by ZCS. (h) TCS forward response comparison.**

(see Fig. 5(f) and Fig. 5(g)). The inverted model obtained by using the forwards from the network trained on TCS also agrees with the synthetic model down to 70-80 m as shown in Fig. 8(d). However, the lower divergence is observed at deeper layers (after 80 m) as compared to the model retrieved from ZCS in relation to the synthetic model. This is because the TCS performs better than ZCS at late times, especially from 100 μs to 1 ms (see Fig. 5(h)). This behavior is observed for other resistivity models in the data set as well. We also show the visual comparison of numerical forward responses with the neural network based forwards of the inverted models for SMMCS, GWMMS, ZCS and TCS in Fig. 8(e-h). The inset in Fig. 8(e-h) shows the forward response comparison from 1 ms to 2 ms for clear visualization of the differences between the numerical and neural network forward responses with the synthetic data.

A. DISCUSSION

The effect of various pre-processing techniques is evaluated for the ground-based tTEM system in this study. Since the tTEM has an offset configuration, the TEM signal is affected by the distance between the transmitter and receiver coil. Therefore, it is considered an input parameter for our neural network which is evident from (3). For other TEM systems, e.g. the airborne SkyTEM, the flight-height affects the signal differently. Therefore, the same analysis needs to be repeated based on the guidelines defined in this article.

Some pre-processing methods may achieve better performance levels as compared to the proposed techniques, however, as long as the guidelines that are defined in this study are followed, the efficiency and performance of the neural network can be ensured. As one of the main takeaways of this investigation is that increased variation in data curves results in improved performance, one can have a substantial indication of the best pre-processing method without training networks with arbitrary pre-processing techniques. It is shown in Fig. 1 and Fig. 5 that each pre-processing method affects the data curves differently, and one method can increase the variation in the curves more than the others.

It can also be observed that all the pre-processed data curves and the network inputs are scaled in the same range i.e. $[-1, 1]$. This is intended for faster approaching to global minima at error surface. However, this might restrict the applicability of our neural network based forward modelling since the pre-processing ties the network and its inputs to the resistivity values in the training set. We expect that it would not significantly affect its extension to other geological settings as the minimum and maximum resistivity values in the training set are encountered to be 0.45 Ω·m and 2275 Ω·m respectively. For TEM systems, it is rare to encounter very conductive environments, i.e. < 0.5 Ω·m. For highly resistive subsurface structures, i.e. by and large > 1000 Ω·m, the TEM method suffers in resolving such layers due to inherent limitations of the method itself. Nevertheless, it could be beneficial to unbind the lower and upper bound of resistivity, which may be achieved at the cost of additional training time once the optimal network architecture is realized.

A network with a single fully-connected hidden layer that is used in this study can approximate any function that contains a continuous mapping from one finite space to another. However, a network with two or three hidden layers may be required to realize the optimal network configuration, since a network with two hidden layers can represent an arbitrary decision boundary to arbitrary accuracy and can approximate any smooth mapping to any accuracy [34]. As smooth mapping may be required, a network with two hidden layers might result in better accuracy performance. However, deciding the number of hidden layers is only a small part of the problem. It is also essential to determine the number of neurons in each of the hidden layers. Several rules of thumb for choosing the number of neurons have been suggested in literature [35]–[38]. These rules of thumb cannot be generalized because they are not always valid for all training cases. Several factors including the network architecture, the degree of noise, the number of hidden layers, and the complexity of the function must be taken into account when selecting the number of neurons. Ultimately, the selection of an architecture for the neural network comes down to trial and error. As mentioned earlier, the purpose of this study is performance comparison between different pre-processing techniques. Therefore, realizing the optimal network configuration is beyond the scope of this work. However, grid search is one of the ways to find the best network configuration.

Other network types including convolutional neural networks, and recurrent neural networks might also be effective for the problem in hand. Since data pre-processing is a critical component in the success of any neural network, it can be expected that other types of neural network would also benefit from an optimal pre-processing strategy.

Once a suitable network architecture is defined, it is instrumental that the training resistivity structures cover the entire model range to achieve acceptable accuracy performance for various geological settings. Currently, the model space covers Danish geological environments. Hence, satisfactory performance can only be expected for such geological structures. In order to cover the entire model range, one way is to augment the training models by shifting the existing resistivity structures by a factor. Another way is to generate random models to cover the entire model range. However, in our experience, using random models for the training of the network does not result in optimal performance for real geological models. Therefore, it is desirable to train the neural network on realistic geological structures.

We used a GA based inversion strategy to show the effect of forward modelling accuracy for TEM inversion. However, a fast and accurate neural network emulator of the forward problem can also be integrated into the gradient-based inversion schemes where the fast forwards can be used to approximate the derivatives for calculating the Jacobian matrix by a first-order difference approach to accelerate inverse modelling. Other Bayesian inversion frameworks that require many forward responses could also significantly benefit from the neural network forwards.

The proposed study is based on the 1-D earth model. Although some of the concepts may be applicable to 3-D modelling, the extension is not trivial and may be considered in the future.

IV. CONCLUSION

We evaluated the effects of several pre-processing methods for the approximation of tTEM forward modelling using neural networks. Numerous experiments showed that the choice of data pre-processing significantly affects the performance of a neural network. The results showed that the gate-wise min-max scaling achieves an accuracy of 95.9% and time-based curve scaling results in 87.3% of all gates within a 3% relative error. The pre-processing technique based on the commonly used logarithmic transform in geophysics domain only achieves an accuracy of 75.0% of all gates within the 3% relative error. The accuracy of these pre-processing methods is superior to the logarithmic transform scaling. We also established the effect of data variation on the performance of our neural network and showed that more variation in data curves consequently results in better performance. Although we have considered the tTEM system, the findings of this study are also applicable to other airborne or ground-based TEM systems.

REFERENCES

[1] M. Shahriaria, D. Pardob, and B. Mosera, "A deep neural network as surrogate model for forward simulation of borehole resistivity measurements," 2019, *arXiv:1910.0255*. [Online]. Available: https://arxiv.org/abs/1910.0255

[2] M. R. Asif, T. S. Bording, A. S. Barfod, B. Zhang, J. J. Larsen, and E. Auken, "Improving computational efficiency of forward modelling for ground-based time-domain electromagnetic data using neural networks," in *Proc. EGU Gen. Assem.*, Vienna, Austria, 2020, p. 7067.

[3] D. Moghadas, A. A. Behroozmand, and A. V. Christiansen, "Soil electrical conductivity imaging using a neural network-based forward solver: Applied to large-scale Bayesian electromagnetic inversion," *J. Appl. Geophys.*, vol. 176, May 2020, Art. no. 104012.

[4] H. Fu, Y. Zhang, and M. Ma, "Seismic waveform inversion using a neural network-based forward," *J. Phys., Conf. Ser.*, vol. 1324, Oct. 2019, Art. no. 012043.

[5] V. Das, A. Pollack, U. Wollner, and T. Mukerji, "Effect of rock physics modeling in impedance inversion from seismic data using convolutional neural network," in *Proc. 13th SEGJ Int. Symp.*, Tokyo, Japan, Apr. 2019, pp. 522–525.

[6] F.-B. Jiang, Q.-W. Dai, and L. Dong, "Nonlinear inversion of electrical resistivity imaging using pruning Bayesian neural networks," *Appl. Geophys.*, vol. 13, no. 2, pp. 267–278, Jun. 2016.

[7] R. Li, H. Zhang, N. Yu, R. Li, and Q. Zhuang, "A fast approximation for 1-D inversion of transient electromagnetic data by using a back propagation neural network and improved particle swarm optimization," *Nonlinear Processes Geophys.*, vol. 26, no. 4, pp. 445–456, Nov. 2019.

[8] V. Puzyrev, S. Meka, and A. Swidinsky, "Deep convolutional neural networks for 1D inversion of electromagnetic data," in *Proc. 81st EAGE Conf. Exhib.*, 2019, pp. 1–5.

[9] D. Moghadas, "One-dimensional deep learning inversion of electromagnetic induction data using convolutional neural network," *Geophys. J. Int.*, vol. 222, no. 1, pp. 247–259, Jul. 2020.

[10] D. Conway, B. Alexander, M. King, G. Heinson, and Y. Kee, "Inverting magnetotelluric responses in a three-dimensional Earth using fast forward approximations based on artificial neural networks," *Comput. Geosci.*, vol. 127, pp. 44–52, Jun. 2019.

[11] S. Bhanja and A. Das, "Impact of data normalization on deep neural network for time series forecasting," 2018, *arXiv:1812.05519*. [Online]. Available: http://arxiv.org/abs/1812.05519

[12] C. Flexa, W. Gomes, and C. Sales, "Data normalization in structural health monitoring by means of nonlinear filtering," in *Proc. 8th Brazilian Conf. Intell. Syst.*, Oct. 2019, pp. 204–209.

[13] J. Sola and J. Sevilla, "Importance of input data normalization for the application of neural networks to complex industrial problems," *IEEE Trans. Nucl. Sci.*, vol. 44, no. 3, pp. 1464–1468, Jun. 1997.

[14] G.-D. Wu and S.-L. Lo, "Effects of data normalization and inherent-factor on decision of optimal coagulant dosage in water treatment by artificial neural network," *Expert Syst. Appl.*, vol. 37, no. 7, pp. 4974–4983, Jul. 2010.

[15] Q. Zhang and S. Sun, "Weighted data normalization based on eigenvalues for artificial neural network classification," in *Proc. Int. Conf. Neural Inf. Process.*, 2009, pp. 349–356.

[16] M. Nabighian, *Electromagnetic Methods in Applied Geophysics*, vol. 1. Tulsa, OK, USA: Society of Exploration Geophysicists, 1988.

[17] E. Auken, N. Foged, J. J. Larsen, K. V. T. Lassen, P. K. Maurya, S. M. Dath, and T. T. Eiskjær, "tTEM—A towed transient electromagnetic system for detailed 3D imaging of the top 70 m of the subsurface," *Geophysics*, vol. 84, no. 1, pp. E13–E22, Jan. 2019.

[18] P. K. Maurya, A. V. Christiansen, J. Pedersen, and E. Auken, "High resolution 3D subsurface mapping using a towed transient electromagnetic system-tTEM: Case studies," *Near Surf. Geophys.*, vol. 18, no. 3, pp. 249–259, Jun. 2020.

[19] A. A. Behroozmand, E. Auken, and R. Knight, "Assessment of managed aquifer recharge sites using a new geophysical imaging method," *Vadose Zone J.*, vol. 18, no. 1, pp. 1–13, Jan. 2019.

[20] H. Kim, A.-S. Høyer, R. Jakobsen, L. Thorling, J. Aamand, P. K. Maurya, A. V. Christiansen, and B. Hansen, "3D characterization of the subsurface redox architecture in complex geological settings," *Sci. Total Environ.*, vol. 693, Nov. 2019, Art. no. 133583.

[21] E. Auken, A. V. Christiansen, C. Kirkegaard, G. Fiandaca, C. Schamper, A. A. Behroozmand, A. Binley, E. Nielsen, F. Effersø, N. B. Christensen, K. Sørensen, N. Foged, and G. Vignoli, "An overview of a highly versatile forward and stable inverse algorithm for airborne, ground-based and borehole electromagnetic and electric data," *Explor. Geophys.*, vol. 46, no. 3, pp. 223–235, Sep. 2015.

[22] S. Theodoridis and K. Koutroumbas, *Pattern Recognition*. New York, NY, USA: Academic, 2009.

[23] B. C. Csáji, "Approximation with artificial neural networks," Dept. Sci., Eötvös Loránd Univ., Budapest, Hungary, 2001, vol. 24, no. 48.

[24] H. Yu, D. C. Samuels, Y.-Y. Zhao, and Y. Guo, "Architectures and accuracy of artificial neural network for disease classification from omics data," *BMC Genomics*, vol. 20, no. 1, p. 167, Dec. 2019.

[25] D. Nguyen and B. Widrow, "Improving the learning speed of 2-layer neural networks by choosing initial values of the adaptive weights," in *Proc. Int. Joint Conf. Neural Netw. (IJCNN)*, 1990, pp. 21–26.

[26] U. Andayani, E. B. Nababan, B. Siregar, M. A. Muchtar, T. H. Nasution, and I. Siregar, "Optimization backpropagation algorithm based on Nguyen–Widrom adaptive weight and adaptive learning rate," in *Proc. 4th Int. Conf. Ind. Eng. Appl. (ICIEA)*, Apr. 2017, pp. 363–367.

[27] K. Mishra, N. Mittal, and M. H. Mirja, "Image compression using multilayer feed forward artificial neural network with Nguyen Widrow weight initialization method," *Int. J. Emerg. Technol. Adv. Eng.*, vol. 4, no. 4, pp. 1–6, 2014.

[28] M. F. Møller, "A scaled conjugate gradient algorithm for fast supervised learning," *Neural Netw.*, vol. 6, no. 4, pp. 525–533.

[29] A. V. Joshi, "Perceptron and neural networks," in *Machine Learning and Artificial Intelligence*. Cham, Switzerland: Springer, 2020, pp. 43–51, doi: 10.1007/978-3-030-26622-6_5.

[30] J. Park and I. W. Sandberg, "Universal approximation using radial-basis-function networks," *Neural Comput.*, vol. 3, no. 2, pp. 246–257, Jun. 1991.

[31] K. Kwan, A. Prikhodko, J. M. Legault, G. Plastow, J. Xie, and K. Fisk, "Airborne inductive induced polarization chargeability mapping of VTEM data," *ASEG Extended Abstr.*, vol. 2015, no. 1, pp. 1–5, 2015.

[32] M. Mitchell, *An Introduction to Genetic Algorithms*. Cambridge, MA, USA: MIT Press, 1998.

[33] S. Raghavan, P. K. Imbrie, and W. A. Crossley, "Spectral analysis of R-lines and vibronic sidebands in the emission spectrum of ruby using genetic algorithms," *Appl. Spectrosc.*, vol. 62, no. 7, pp. 759–765, Jul. 2008.

[34] J. Heaton, *Introduction to Neural Networks With Java*. St. Louis, MO, USA: Heaton Research, 2008.

[35] E. K. Blum and L. K. Li, "Approximation theory and feedforward networks," *Neural Netw.*, vol. 4, no. 4, pp. 511–515, Jan. 1991.

[36] M. J. Berry and G. Linoff, *Data Mining Techniques: For Marketing, Sales, and Customer Support 1997*. Hoboken, NJ, USA: Wiley, 1997.

[37] Z. Boger and H. Guterman, "Knowledge extraction from artificial neural network models," in *Proc. IEEE Int. Conf. Syst., Man, Cybern. Comput. Cybern. Simulation*, Oct. 1997, pp. 3030–3035.

[38] J. Ke and X. Liu, "Empirical analysis of optimal hidden neurons in neural network modeling for stock prediction," in *Proc. IEEE Pacific–Asia Workshop Comput. Intell. Ind. Appl.*, Dec. 2008, pp. 828–832.

MUHAMMAD RIZWAN ASIF received the B.S. degree in electrical (telecommunication) engineering from COMSATS University Islamabad (CUI), in 2013, and the M.S. and Ph.D. degrees in information and communication engineering from Xi'an Jiaotong University, in 2016 and 2019, respectively.

Since 2019, he has been holding a postdoctoral position with the Department of Electrical and Computer Engineering, Aarhus University, Denmark. He is currently working in close collaboration with the Hydrogeophysics Group (HGG), Department of Geoscience, Aarhus University, to support research projects employing electrical and electromagnetic methods. His current research interests include machine learning applications for geophysical data, image processing, and computer vision for intelligent automated systems.

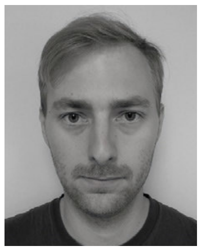

THUE S. BORDING received the B.Sc. degree in geology from Aarhus University, in 2010, and the Ph.D. degree in geophysics (geothermal modelling and measurement of rock thermal properties) in 2016. Since 2016, he has been holding a postdoctoral position with the Hydrogeophysics Group (HGG), Department of Geoscience, Aarhus University. His current research interests include cross-borehole electrical tomography, induced polarization, and transient electromagnetics.

ADRIAN S. BARFOD received the B.Sc. degree in geology from the Department of Geoscience, Aarhus University, in 2012, and the master's degree in 2013. In 2013, during his master's program, he was accepted as a Ph.D. student at the Geological Survey of Denmark and Greenland (GEUS) and the Hydrogeophysics Group (HGG), Department of Geoscience, Aarhus University. In 2017, he graduated from Aarhus University with the thesis title "Investigating Lithological and Geophysical Relationships With Applications to Geological Uncertainty Analysis Using Multiple-Point Statistical Methods." He currently holds a postdoctoral position with the Department of Electrical and Computer Engineering, Aarhus University.

DENYS J. GROMBACHER received the B.Sc. degree in astrophysics from the University of Alberta, in 2010, and the Ph.D. degree in geophysics from Stanford University, in 2015. His research interests include electromagnetic and nuclear magnetic resonance technologies for groundwater explorations.

PRADIP K. MAURYA received the Ph.D. degree in direct current resistivity and induced polarization (DCIP) method in 2017. He currently holds a postdoctoral position with the Hydro Geophysics Group, Aarhus University. Apart from DCIP method, his research interests include airborne and ground-based electromagnetic methods for near surface applications, data processing, the inversion of electromagnetic data, the development of geophysical instruments, and the development of tTEM instrument.

ANDERS V. CHRISTIANSEN received the Ph.D. degree within airborne TEM methods and inversion methodologies in 2003. He is currently an Associate Professor with the Hydrogeophysics Group, Aarhus University, Denmark. His research interest includes the integration of various data types (e.g., geophysics with borehole information and hydrological observations) with the purpose of making objective and transparent processes that generate maps and other outputs that are in better agreement with the actual needs of the end-users.

ESBEN AUKEN received the M.Sc. and Ph.D. degrees in geophysics from Aarhus University, in 1991 and 1996, respectively. He was a Professor of geophysics with the Department of Geoscience, Aarhus University, Denmark. During his affiliation with Aarhus University, he led a big research team (The Hydrogeophysics Group, HGG) consisted of 25–30 scientists all working with electrical and electromagnetic methods for high resolution mapping of the shallow subsurface with focus on surface and groundwater processes. HGG does high-level research on instrumental engineering, data processing and high performance 1D, 2D, and 3D inversion algorithms. Hydrological modeling with extensive input from areal-covering geophysical measurements is an integrated part of the research. He is currently the Vice Director of the Geological Survey of Denmark and Greenland (GEUS). GEUS carries out activities to explore and protect geological resources in Denmark and Greenland. He is also a Co-Founder of SkyTEM Surveys Aps, Aarhus Geo-Software, and Aarhus Geo-Instruments, all spin-out companies from the research group. The geophysical focus areas are surface nuclear magnetic resonance (NMR), ground-based and airborne transient electromagnetics, and surface and cross borehole direct current and induced polarization. In addition, he has taught short and academic courses for professionals and for bachelor's and master's students. His research interests include mapping, compilation, and storage of data, research, monitoring and consultancy within water, energy, minerals, and climate and environment.

JAKOB J. LARSEN (Senior Member, IEEE) was born in Denmark in 1973. He received the M.Sc. and Ph.D. degrees in experimental physics from Aarhus University, Denmark, in 1998 and 2000, respectively. From 2000 to 2013, he held research and teaching positions in private and public companies. Since 2013, he has been with the Department of Electrical and Computer Engineering, Aarhus University, where he is currently an Associate Professor. He also works with geophysical instrumentation, signal processing, and machine learning. His current research interests include the domains of magnetics, transient electromagnetics, direct current induced polarization, and surface nuclear magnetic resonance.